

# DETECT EVERY THING WITH FEW EXAMPLES

Xinyu Zhang, Yuting Wang & Abdeslam Boularias

Department of Computer Science

Rutgers University

{xz653, yw632, ab1544}@rutgers.edu

## ABSTRACT

Open-set object detection aims at detecting arbitrary categories beyond those seen during training. Most recent advancements have adopted the open-vocabulary paradigm, utilizing vision-language backbones to represent categories with language. In this paper, we introduce DE-ViT, an open-set object detector that employs vision-only DINOv2 backbones and learns new categories through example images instead of language. To improve general detection ability, we transform multi-classification tasks into binary classification tasks while bypassing per-class inference, and propose a novel region propagation technique for localization. We evaluate DE-ViT on open-vocabulary, few-shot, and one-shot object detection benchmark with COCO and LVIS. For COCO, DE-ViT outperforms the open-vocabulary SoTA by 6.9 AP50 and achieves 50 AP50 in novel classes. DE-ViT surpasses the few-shot SoTA by 15 mAP on 10-shot and 7.2 mAP on 30-shot and one-shot SoTA by 2.8 AP50. For LVIS, DE-ViT outperforms the open-vocabulary SoTA by 2.2 mask AP and reaches 34.3 mask APr. Code is available at <https://github.com/mlzxy/devit>.

## 1 INTRODUCTION

Object recognition and localization are two of the core tasks in computer vision. In this work, we present a novel generic object detector that detects objects of arbitrary categories, a paradigm commonly referred to as *open-set object detection*<sup>1</sup>. Following recent advances in vision-language models (Radford et al., 2021), *open-vocabulary object detection* achieved a remarkable success by representing each class with language embeddings of its category names (Zhong et al., 2022). However, we argue that there exist fundamental limitations in using language for category representation. First, certain objects are difficult to accurately describe with only language, or lack concise denomination (Landau et al., 2009; Pires et al., 2019). Second, the association between visual concepts and language is constantly evolving and not static (Dorogovtsev & Mendes, 2001), while an open-vocabulary model can only link objects and names that were previously connected in the corpus. Third, language-based categorization does not exploit image annotations when they are available.

*Few-shot object detection*, albeit receiving far less recent research attention, directly uses images instead of language to describe categories, bypassing the above limitations. However, most recent few-shot methods focus on finetuning-based strategies (Köhler et al., 2023), which requires further training on the novel categories, a complicated and tedious procedure that restricts the practical use of these methods (Zhao et al., 2022b). Moreover, despite overcoming these limitations in principle, the accuracy of few-shot methods falls behind that of the open-vocabulary solutions in practice, especially in large-scale datasets such as COCO and LVIS (Ma et al., 2023; Wu et al., 2023c).

In this paper, we introduce DE-ViT, an open-set object detector that uses representative images to categorize objects. We adopt an RCNN framework (Girshick, 2015) and use pretrained vision-only backbones, specifically DINOv2 ViT (Oquab et al., 2023), to extract image features and build prototype vectors, *i.e.*, class representatives. We use off-the-shelf region proposal networks (RPN) and design novel classification and refined localization architectures for generic object detection,

<sup>1</sup>Some recent studies use *open-set* as a synonym for *open-vocabulary*, whereas we view *open-set object detection* as the general objective, *i.e.*, the capability to detect objects of arbitrary classes. Both *open-vocabulary* and *few-shot* belong to *open-set* except their category representations, *i.e.*, language versus images.

which exclusively relies on similarity maps between image features and the constructed prototypes. New classes can be added with a few example images in an ad-hoc manner without any finetuning. The DINOv2 backbones are kept frozen and only our detection-related layers are trained. The overall architecture is illustrated in Fig. 2. A demonstration of detecting YCB objects is shown in Fig. 1.



Figure 1: Demonstration of the proposed method on YCB objects (Calli et al., 2015). DE-ViT with ViT-L/14 is used for prediction. Note that our model is trained on only the base categories of LVIS. Example images of YCB objects are provided only during inference to represent novel categories.

We evaluate DE-ViT on open-vocabulary, few-shot, and one-shot object detection benchmarks with COCO (Lin et al., 2014) and LVIS (Gupta et al., 2019) datasets. Our method establishes new state-of-the-art (SoTA) results on all benchmarks. For COCO, DE-ViT outperforms the existing open-vocabulary SoTA CORA<sup>+</sup> (Wu et al., 2023c) by 6.9 AP50 and establishes a new SoTA at 50 AP50. DE-ViT surpasses the few-shot SoTA LVC (Kaul et al., 2022) by 15 mAP on 10-shot and 7.2 mAP on 30-shot and one-shot SoTA BHRL (Yang et al., 2022) by 2.8 AP50. For LVIS, DE-ViT outperforms the open-vocabulary SoTA Ro-ViT (Kim et al., 2023) by 2.2 mask AP, reaching 34.3 mask AP in novel categories. Our method only trains on the corresponding dataset, i.e., COCO or LVIS, without leveraging extra datasets for training, or distillation. Our contributions are summarized as follows: (1) We show and verify the potential of employing images as category representations for performing open-set object detection. (2) We introduce DE-ViT, an example-driven open-set object detector based on frozen vision-only DINOv2 backbones. (3) We demonstrate that DE-ViT establishes state-of-the-art performance over open-vocabulary, few-shot, and one-shot benchmarks on both COCO and LVIS.

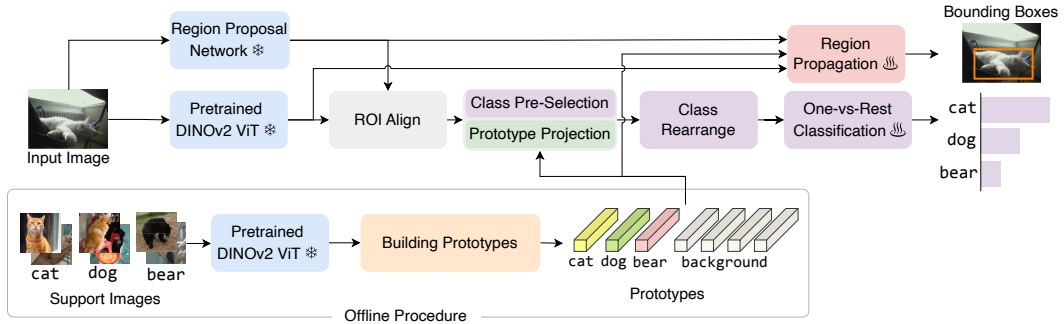


Figure 2: Overview of the proposed method. Our approach uses DINOv2 ViT to encode the image into a feature map, from which proposal features are extracted using ROIAlign. Proposals are generated via an off-the-shelf RPN. Prototype projection transforms proposal features into similarity maps based on prototypes derived from ViT features of support images. Multi-class classification of proposals is recast as a series of one-vs-rest binary classification tasks without the need for costly per-class inference. Refined localization is accomplished by our novel region propagation module. Both classification and refined localization rely exclusively on the computed similarity maps.

## 2 RELATED WORK

**Few-shot Object Detection (FSOD)** aims at detecting objects of novel classes by utilizing a few support images from novel classes as training examples (Köhler et al., 2023). Existing approaches can be broadly classified into finetuning-based (Wang et al., 2020; Fan et al., 2021; Sun et al., 2021; Xiao et al., 2022; Kaul et al., 2022; Ma et al., 2023; Guirguis et al., 2023) and meta-learning-based strategies (Yan et al., 2019; Han et al., 2021; 2022b;a). Finetuning-based methods, despite their prevalence, suffer from a large accuracy gap between the base and the novel classes, as well as practical limitations due to redundant two-stage procedures (Zhao et al., 2022b). Meta-learning methods avoid finetuning by online adaptation, but exhibit inferior accuracy (Köhler et al., 2023). One-shot Object Detection (OSOD) is an extreme case of FSOD with only one exemplar for each novel class. OSOD simplifies the setting to single-class detection without finetuning. Prior approaches primarily focus on designing interaction mechanisms of dense spatial features between support and target images (Antonelli et al., 2022). However, the OSOD formulation restricts the use of additional support, if available, and requires a separate inference per class. Compared with existing work, our method does not use finetuning or per-class inference, and only utilizes class-level prototypes without dense feature interactions, while outperforming SoTA methods in both few-shot and one-shot settings.

**Open-Vocabulary Object Detection (OVD)** aims at detecting objects of novel classes based on their category names (Zareian et al., 2021). The prevalent paradigm generally consists of two stages: image-text pretraining and downstream detector training. OWL-ViT (Minderer et al., 2022) and Ro-ViT (Kim et al., 2023) redesign the first stage for OVD tasks and do not rely on publicly available models. Due to the high computational cost of the initial stage, building such a framework can be challenging. RegionCLIP (Zhong et al., 2022) and VL-PLM (Zhao et al., 2022a) propose image-text finetuning with pseudo bounding boxes to enhance the alignment between image regions and text features. CORA (Wu et al., 2023c) introduces region prompting techniques as an alternative to full finetuning. Detic (Zhou et al., 2022b) and MEDet (Chen et al., 2022) blur the boundaries between the two stages by simultaneously training on both image-text pairs and bounding boxes. ViLD (Gu et al., 2021) and BARON (Wu et al., 2023b) focus on the downstream detector training with distillation. OV-DETR (Zang et al., 2022) proposes DETR-based detectors (Carion et al., 2020) but suffers from inefficient per-class inference. Compared with OVD methods, we represent each class with a prototype vector derived from support images instead of a text embedding vector. Our method surpasses state-of-the-art OVD methods on both LVIS and COCO. Remarkably, we achieve these results by designing a novel architecture on top of frozen pretrained DINOv2 backbones without employing any form of distillation or alignment training.

## 3 METHOD

The major challenge in both FSOD and OVD is to generalize to classes that are unseen during training. However, despite numerous attempts to address this issue, through margin-based regularization (Ma et al., 2023) or extra supervision from captions (Zhou et al., 2022b), for example, there still persists a considerable accuracy gap between base and novel classes. This disparity indicates that a network trained with base classes would inevitably fixate on patterns that are only present among a few base classes, which does not align with the objective of detecting arbitrary classes.

To address this challenge, we propose to learn not only backbone features, but also maps of similarities between the features and a set of prototypes. Specifically, let  $\mathbf{f} \in \mathbb{R}^{H \times W \times D}$  be the features of an image where  $D$  represents the channel dimension and  $(H, W)$  represent spatial dimensions, let  $\mathbf{p} \in \mathbb{R}^{(C+B) \times D}$  be the prototypes where  $C$  is the number of classes and  $B$  is the number of class-agnostic background prototypes. Similarity map  $\mathbf{s} \in \mathbb{R}^{H \times W \times (C+B)}$  is calculated using Eq. 1. This procedure is referred to in Fig. 3 as prototype projection. We use  $[C + B]$  to denote  $\{1, \dots, C + B\}$ .

$$\mathbf{s}_{ijc} = \sum_{d=1}^D \mathbf{f}_{ijd} \mathbf{p}_{cd}, \text{ where } (i, j, c) \in [H] \times [W] \times [C + B] \quad (1)$$

We adopt a standard two-stage object detection framework, *e.g.*, Mask R-CNN (He et al., 2017), which detects objects through RPN and RCNN stages. Existing literature has demonstrated that class-agnostic RPN proposals generalize well to novel classes (Gu et al., 2021). We use off-the-shelf RPNs to propose object regions and extract proposal features from DINOv2 ViT backbones.

Similarity maps are computed between proposal features and prototypes, which are then fed to our architectures for classification and refined localization. Prototypes are constructed offline from support images with the procedures detailed in Sec. 3.3. The ViT backbones, prototypes, and resulting the similarity maps are kept frozen during detector training.

### 3.1 CLASSIFICATION WITH AN UNKNOWN NUMBER OF CLASSES

Unlike supervised learning, the number of classes in FSOD and OVD is indeterminate. The common strategy in FSOD is to extend the final linear layer with finetuning. The prevailing practice in OVD is to compose the last linear layer with text embedding vectors of category names (Wu et al., 2023a). In contrast with these existing approaches, we transform the multi-classification of  $C$  classes into  $C$  one-vs-rest binary classification tasks. The overall classification architecture is illustrated in Fig. 3.

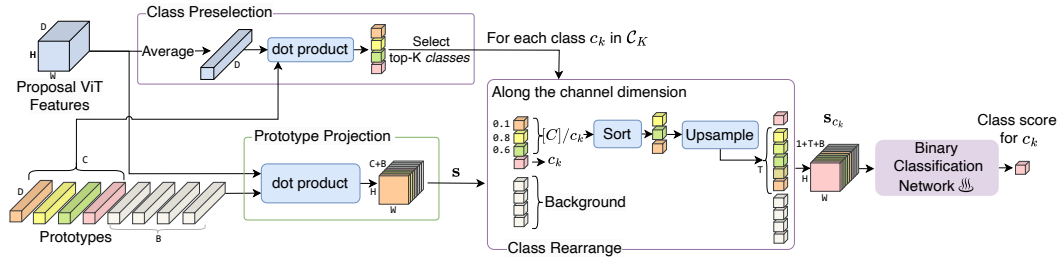


Figure 3: Overview of our classification architecture. Class pre-selection chooses the top- $K$  classes based on the dot product similarity between the average feature of each proposal and class-level prototypes. The class score of each selected class  $c_k$  is predicted through a binary classification network, shared by all the classes, in a one-vs-rest manner. The input to this classification network is the similarity map that results from the prototype projection, after rearranging it for each class.

Let  $\bar{\mathbf{f}} = \frac{\sum_{i,j=1}^{H,W} \mathbf{f}_{ij}}{HW} \in \mathbb{R}^D$  be the average feature of a proposal. The class pre-selection procedure returns the top- $K$  mostly likely classes  $\mathcal{C}_K = \text{top\_indices}_K(\mathbf{h})$ .  $\mathbf{h} \in \mathbb{R}^C$  is the dot-product similarity between  $\bar{\mathbf{f}}$  and class prototypes, defined as  $\mathbf{h}_c = \sum_{d=1}^D \bar{\mathbf{f}}_d \mathbf{p}_{cd}, \forall c \in [C]$ . The average feature  $\bar{\mathbf{f}}$  is only used to select top classes  $\mathcal{C}_K$ . For each class  $c_k$  in  $\mathcal{C}_K$ , the similarity map  $\mathbf{s} \in \mathbb{R}^{H \times W \times (C+B)}$  (computed in Eq. 1) is rearranged into a class-specific map  $\mathbf{s}_{c_k} \in \mathbb{R}^{H \times W \times (1+T+B)}$ , which consists of the similarities between the input image’s features and the prototype for  $c_k$ , as well as the prototypes for the classes in  $[C]/c_k$ , and the background, as shown in Eq. 2, where  $[C]/c_k$  is defined as  $\{1, \dots, c_k - 1, c_k + 1, \dots, C\}$ .

$$\mathbf{s}_{c_k} = \text{concat}(\mathbf{s}[:, :, c_k], F_{\text{rearrange}}(\mathbf{s}_{[C]/c_k}), \mathbf{s}[:, :, C : C + B]) \quad (2)$$

where  $\mathbf{s}_{[C]/c_k} = \text{concat}(\mathbf{s}[:, :, : c_k - 1], \mathbf{s}[:, :, c_k + 1 :])$ , and  $F_{\text{rearrange}}(\mathbf{x})$  is defined in Eq. 3.  $T$  is a constant hyper-parameter.

$$F_{\text{rearrange}}(\mathbf{x}) = \begin{cases} \text{upsample}(\text{sort}(\mathbf{x}), T) & \text{if } T \geq C - 1 \\ \text{sort}(\mathbf{x})[:, :, : T] & \text{otherwise} \end{cases} \quad (3)$$

$F_{\text{rearrange}}(\mathbf{x})$  first ranks  $[C]/c_k$  by sorting  $\mathbf{s}_{[C]/c_k}$  along the channel dimension in similarity magnitude. Next, either the similarities to the top  $T$  classes are kept or the similarities to all  $C - 1$  classes are linearly upsampled to  $T$ . In doing so,  $\mathbf{s}_{[C]/c_k}$  is transformed from a non-deterministic size of  $H \times W \times (C - 1)$  into a fixed size  $H \times W \times T$ . Note that the listed functions, *i.e.*, sort, concat and upsample, are applied along the channel dimension, and sort works in descending order. Finally, the class-specific similarity map  $\mathbf{s}_{c_k}$  is given as input to a binary classification network that returns the class score for  $c_k$ . Our method only predicts class scores for  $\mathcal{C}_K$  and sets the others to 0. As shown in Sec. 4.2, our method surpasses SoTA even when  $K = 3$  on both COCO (80 classes) and LVIS (1203 classes), eliminating the need for costly per-class inference.

### 3.2 LOCALIZATION WITH REGION PROPAGATION.

Despite their rich semantics information, ViT features lack the coordinates information required for bounding box regression. As shown in Sec. 4.2, naively applying a conventional regression on ViT features yields poor localization results. A natural solution is to learn this localization capability by finetuning the ViT backbone during detector training. This finetuning strategy has demonstrated success in OVD for vision-language backbones, *e.g.*, CLIP (Zhong et al., 2022). However, we observed that finetuning results in an accuracy collapse on novel classes when text embeddings are replaced with prototypes, which indicates a loss of generalization power. While this phenomenon is intriguing, the practical question is how to produce accurate localization using frozen visual features.

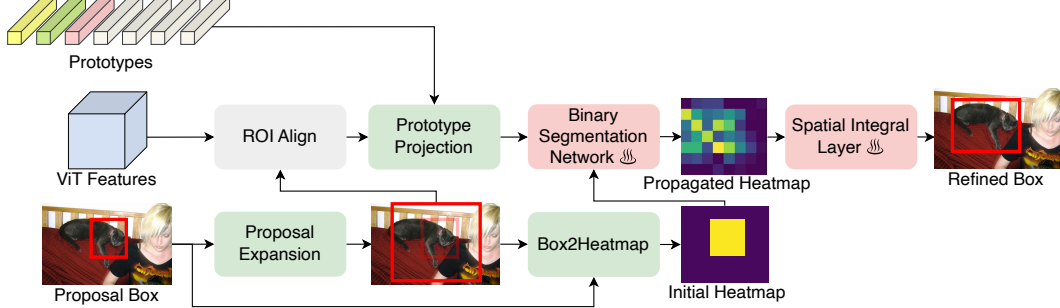


Figure 4: Overview of our refined localization architecture. Proposal expansion enlarges each proposal by a fixed ratio to cover more object area. The spatial relationship between the original and expanded proposal is described via a heatmap. The segmentation network navigates the initial heatmap toward accurate object regions. The propagated heatmap is converted into bounding box coordinates through our spatial integral layer.

Our intuition is that only proposals that overlap with objects are important because others would be rejected by the classification network. If we expand such proposals, they would possibly cover the entire region of underlying objects. Therefore, original proposals can be refined by predicting object regions within the expanded proposals. We model this procedure as propagating original proposals to object areas in the form of heatmaps. The heatmaps can be projected into box coordinates through integral over spatial dimensions. The overall refined localization architecture is illustrated in Fig. 4.

As shown in Fig. 4, the propagation procedure is implemented through binary segmentation. We convert groundtruth bounding boxes to heatmaps that we use to train this segmentation network. Inspired by unsupervised keypoint estimation, particularly the works of IMM (Jakab et al., 2018) and Transporter (Kulkarni et al., 2019), we devise a spatial integral layer to project the propagated heatmap to box. The idea is to learn a transformation that translates the heatmap to a box  $(c_w^{\text{rel}}, c_h^{\text{rel}}, w^{\text{rel}}, h^{\text{rel}}) \in [0, 1]^4$  in coordinates that are relative to the expanded proposal. Relative coordinates can be simply mapped back to absolute coordinates. Let  $\mathbf{g} \in \mathbb{R}^{H \times W}$  denote the logits of the propagated heatmap, the relative box  $(c_w^{\text{rel}}, c_h^{\text{rel}}, w^{\text{rel}}, h^{\text{rel}})$  can be estimated using Eq. 4.

$$\begin{aligned}
 (c_w^{\text{rel}}, c_h^{\text{rel}}) &= \sum_{i,j=1}^{H,W} \left( \frac{i}{H}, \frac{j}{W} \right) * \text{softmax}(\mathbf{g})_{ij} \\
 (w^{\text{rel}}, h^{\text{rel}}) &= \left( \sum_{i=1}^H \sum_{j=1}^W \frac{\sigma(\mathbf{g})_{(i)j}}{W} \theta^w_i, \sum_{j=1}^W \sum_{i=1}^H \frac{\sigma(\mathbf{g})_{i(j)}}{H} \theta^h_j \right)
 \end{aligned} \tag{4}$$

Eq. 4 estimates the box center as the center of the spatial distribution of the propagated heatmap. Note that the softmax is applied over both spatial dimensions. The notation  $\sigma$  represents elementwise sigmoid,  $\theta^h \in \mathbb{R}^W, \theta^w \in \mathbb{R}^H$  are learnable parameters,  $(i)$  and  $(j)$  denote order statistics, *i.e.*,  $\sigma(\mathbf{g})_{i(j)}$  stands for the  $j$ -th largest value at  $i$ -th row of  $\sigma(\mathbf{g})$ . Take  $w^{\text{rel}}$  as an example, the inner summation  $\sum_{j=1}^W \sigma(\mathbf{g})_{(i)j}$  produces a width estimate at each row. Then, the final estimate is the ensemble of row-level estimates weighted by order statistics. The rationale is that a larger estimate

is likely to be located at the object area and therefore matters more. Finally, the relative coordinates are mapped to absolute ones by Eq. 5, where  $(c_w^{\text{exp}}, c_h^{\text{exp}}, w^{\text{exp}}, h^{\text{exp}})$  is the expanded proposal.

$$\begin{aligned} (w^{\text{out}}, h^{\text{out}}) &= (w^{\text{exp}} w^{\text{rel}}, h^{\text{exp}} h^{\text{rel}}) \\ (c_w^{\text{out}}, c_h^{\text{out}}) &= (c_w^{\text{exp}} - 0.5w^{\text{exp}}, c_h^{\text{exp}} - 0.5h^{\text{exp}}) + (c_w^{\text{rel}} w^{\text{exp}}, c_h^{\text{rel}} h^{\text{exp}}) \end{aligned} \quad (5)$$

During training, we use groundtruth bounding boxes as regression targets for the output of spatial integral layer. Similar to our classification pipeline, the localization procedure is applied for each class in  $\mathcal{C}_K$  to produce class-specific boxes. For each class  $c_k$ , only the similarity map of  $c_k$  and the background will be selected as input. We omit this detail in Fig. 4 for visual clarity.

### 3.3 BUILDING PROTOTYPES

While OVD uses text embeddings of category names to represent classes, our method represents classes with prototype vectors constructed from visual features of given support images. Fig. 5 shows the process of building instance-level prototypes. For each object instance, its prototype is computed as the mean ViT feature from corresponding regions defined by either a segmentation mask or bounding box. Next, class-representing prototypes are obtained by averaging the cluster centroids of instance-level prototypes for each class. We use the online clustering method proposed by SwAV (Caron et al., 2020), though we find that simply averaging all instance prototypes for each class achieves similar results. Prototypes of base classes are built from the entire training set instead of support images, which are used only for novel classes.

To build background prototypes, we start from the observation that backgrounds typically share similar visual attributes, such as uniform motion, smooth texture, static color tone, *etc.* Moreover, the ability to capture and thereby separate background from foreground is crucial. Because of the lack of visual diversity yet the importance of background semantics, we use masks for a fixed list of background classes, *e.g.*, sky, wall, road, and apply a similar prototype-building procedure. The idea of using background information for few-shot performance is similarly explored in IPRNet (Okazawa, 2022). In contrast with class-level prototypes that change upon class configurations, background prototypes are always fixed as a part of the network’s parameters. All the prototypes are built offline and frozen during training and inference.

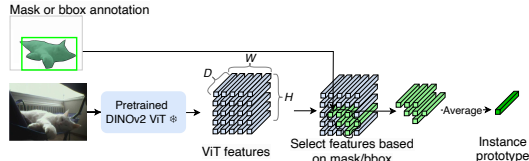


Figure 5: Overview of building instance prototypes.

Figure 5: Overview of building instance prototypes. The idea of using background information for few-shot performance is similarly explored in IPRNet (Okazawa, 2022). In contrast with class-level prototypes that change upon class configurations, background prototypes are always fixed as a part of the network’s parameters. All the prototypes are built offline and frozen during training and inference.

## 4 EXPERIMENTS

We comprehensively evaluate our method on few-shot, one-shot, and open-vocabulary object detection benchmarks. Furthermore, we compare the efficiency of our method against SoTA solutions and conduct ablations to study different components of the proposed technique.

**Datasets and Evaluation.** For open-vocabulary detection, we evaluate our method on COCO-2017 (Lin et al., 2014) and LVIS-v1 (Gupta et al., 2019). Following the convention (Zhong et al., 2022), the 80 classes of COCO are divided into 48 base classes and 17 novel classes. On LVIS, 866 common categories are used for base classes and 337 rare categories are novel classes. We report AP50 for COCO, and both mask and box AP for LVIS. Unlike most existing OVD work, our method does not require extra data for multi-stage pretraining or distillation. For few-shot learning, we evaluate on COCO-2014 and LVIS-v1. The 80 classes of COCO are divided into 60 base classes and 20 novel classes. LVIS shares the same base/novel split between OVD and FSOD (Wang et al., 2020). We report mAP, AP50, and AP75. For one-shot learning, we follow the convention (Yang et al., 2022) to equally split the 80 classes of COCO-2017 into four parts and alternately take three parts (60 classes) as base classes and one part (20 classes) as novel classes, and we report AP50.

**Model Specifications.** We use DINOv2 (Oquab et al., 2023) ViT as the feature extractor, and report results in ViT-S/B/L (small, base, large) model sizes. We train a ResNet50 RPN separately for each dataset configuration using only base classes and use 1000 proposals in all settings. We

Table 1: Results on COCO OVD benchmark. We report AP50 as the evaluation metric and list the extra dataset requirement. †: Customized pretrained model is used instead of public models.

| Method                          | Backbone  | Use Extra Training Set | Generalized (17 + 48) |      |      |
|---------------------------------|-----------|------------------------|-----------------------|------|------|
|                                 |           |                        | Novel                 | Base | All  |
| OVR-CNN (Zareian et al., 2021)  | RN50      | ✓                      | 22.8                  | 46.0 | 39.9 |
| ViLD (Gu et al., 2021)          | ViT-B/32  | ✗                      | 27.6                  | 59.9 | 51.3 |
| RegionCLIP (Zhong et al., 2022) | RN50x4    | ✓                      | 39.3                  | 61.6 | 55.7 |
| OV-DETR (Zang et al., 2022)     | ViT-B/32  | ✗                      | 29.4                  | 61.0 | 52.7 |
| VL-PLM (Zhao et al., 2022a)     | RN50      | ✗                      | 34.4                  | 60.2 | 53.5 |
| Detic (Zhou et al., 2022b)      | RN50      | ✓                      | 27.8                  | 47.1 | 45.0 |
| MEDet (Chen et al., 2022)       | RN50      | ✓                      | 32.6                  | 54.0 | 49.4 |
| BARON (Wu et al., 2023b)        | RN50      | ✗                      | 34                    | 60.4 | 53.5 |
| Ro-ViT (Kim et al., 2023)       | ViT-L/16† | ✗                      | 33                    | -    | 47.7 |
| CORA (Wu et al., 2023c)         | RN50x4    | ✗                      | 41.7                  | 44.5 | 43.8 |
| CORA+ (Wu et al., 2023c)        | RN50x4    | ✓                      | 43.1                  | 60.9 | 56.2 |
| DE-ViT (Ours)                   | ViT-S/14  | ✗                      | 39.5                  | 42.3 | 41.5 |
|                                 | ViT-B/14  | ✗                      | <b>45.4</b>           | 51.8 | 50.1 |
|                                 | ViT-L/14  | ✗                      | <b>50.0</b>           | 54.0 | 52.9 |

use lightweight CNNs for both binary classification and segmentation networks, which we detail in Sec. A.3. Class prototypes are built upon instance masks in support images unless specified. We use the same support images as sampled by previous work (Wang et al., 2020; Yang et al., 2022) for few-shot and one-shot settings. For the open-vocabulary setting, we sample 30 instances per class (30-shot) using the protocol of Wang et al. (2020). Background prototypes are extracted from background classes, *e.g.*, sky, road, by the semantic masks in COCOStuff (Caesar et al., 2018).

#### 4.1 MAIN RESULTS

Tab. 1 and 2 show our results on open-vocabulary COCO and LVIS. We list whether extra datasets are required for training. DE-ViT outperforms the previous SoTA CORA+ by 6.9 AP50. Our method only trains on COCO while CORA+ uses ImageNet-21K (Krizhevsky et al., 2012) and COCO Captions (Chen et al., 2015) with generated pseudo detection labels as extra datasets. When only using COCO, DE-ViT outperforms CORA by 8.3 AP50. In LVIS, DE-ViT outperforms the previous SoTA on both mask APr (+2.2 over Ro-ViT) and box APr (+2.4 over OWL-ViT). Our method only trains on LVIS and uses frozen public models while OWL-ViT trains on an aggregation of detection datasets, and both Ro-ViT and OWL-ViT train their own ViT backbones with customized vision-language pertaining pipelines. We use “-” to indicate work that does not report mask or box APs. We follow a conventional multi-scale instance segmentation head design, as detailed in Sec. A.3.

Tab. 3 shows our results on few-shot COCO. DE-ViT outperforms the previous SoTA LVC by a significant margin (+15 nAP on 10-shot, +7.2 nAP on 30-shot). nAP represents mAP in novel classes. LVC applies finetuning and pseudo-labeling on novel classes, while our method does not require finetuning. Our method shows no accuracy difference between 10-shot and 30-shot. Tab. 8 shows that similar accuracy can be obtained at even 5-shot. It is possible that the representation power of DINOv2, despite being strong, already saturates upon a few images when using a single prototype per class. LVIS has been regarded as a highly challenging dataset in FSOD (Wang et al., 2020) and only DiGeo reports few-shot results on LVIS v1, the comparison is reported in Appendix Tab. A1 to save space.

Tab. 4 shows our results on one-shot COCO. DE-ViT outperforms the previous SoTA BHRL by 2.8 and 6 AP50 on unseen and seen classes. Note that one-shot detection follows a single-class object detection formulation. We adapt our method to this setting by detecting each class separately. Notice that the gap between seen and unseen classes is much larger in one-shot than few-shot setting. This shows that a single image may be insufficient to describe categories with high intra-variance. OWL-ViT also reports one-shot results on COCO. However, OWL-ViT’s results are obtained with an ensemble of open-vocabulary and one-shot pipelines without providing implementation or isolated measurements. Therefore, we only compare against OWL-ViT in open-vocabulary benchmarks.



Table 2: Results on LVIS OVD benchmark. We report both mask and box AP. \*: Use a larger image size. †: Customized pretrained model is used instead of public models.

| Method                               | Backbone              | Use Extra Training Set | mask AP <sub>r</sub> | box AP <sub>r</sub> | mask AP | box AP |
|--------------------------------------|-----------------------|------------------------|----------------------|---------------------|---------|--------|
| ViLD (Gu et al., 2021)               | EffNet-B7             | ✗                      | 26.3                 | 27                  | 29.3    | 31.8   |
| RegionCLIP (Zhong et al., 2022)      | RN50x4                | ✓                      | -                    | 22                  | -       | 32.3   |
| OV-DETR (Zang et al., 2022)          | ViT-B/32              | ✗                      | -                    | 17.4                | -       | 26.6   |
| VL-PLM (Zhao et al., 2022a)          | RN50                  | ✗                      | -                    | 17.2                | -       | 27.0   |
| Detic (Zhou et al., 2022b)           | RN50                  | ✓                      | 17.8                 | -                   | 26.8    | -      |
| MEDet (Chen et al., 2022)            | RN50                  | ✓                      | 22.4                 | -                   | 34.4    | -      |
| OWL-ViT (Minderer et al., 2022)      | ViT-L/14 <sup>†</sup> | ✗                      | -                    | 25.6                | -       | 34.7   |
| OWL-ViT (Minderer et al., 2022)      | ViT-L/14 <sup>†</sup> | ✓                      | -                    | 31.2                | -       | 34.6   |
| GroundingDINO (Liu et al., 2023)     | Swin-L                | ✓                      | -                    | 22.2                | -       | 33.9   |
| CORA <sup>+</sup> (Wu et al., 2023c) | RN50x4                | ✓                      | -                    | 28.1                | -       | -      |
| PCL (Cho et al., 2023)               | Swin-L                | ✓                      | -                    | 30.6                | -       | 34.5   |
| Ro-ViT (Kim et al., 2023)            | ViT-L/14 <sup>†</sup> | ✗                      | 31.4                 | -                   | 34.0    | -      |
| Ro-ViT (Kim et al., 2023)*           | ViT-L/16 <sup>†</sup> | ✗                      | 32.1                 | -                   | 34.0    | -      |
| DE-ViT (Ours)                        | ViT-S/14              | ✗                      | 24.2                 | 23.4                | 23.1    | 22.8   |
|                                      | ViT-B/14              | ✗                      | 28.5                 | 26.8                | 27.6    | 26     |
|                                      | ViT-L/14              | ✗                      | <b>34.3</b>          | <b>33.6</b>         | 31.5    | 30.9   |

Table 3: Results on COCO few-shot benchmark.

| Method                                | 10-shot  |      |             |             | 30-shot     |      |             |             |             |
|---------------------------------------|----------|------|-------------|-------------|-------------|------|-------------|-------------|-------------|
|                                       | bAP      | nAP  | nAP50       | nAP75       | bAP         | nAP  | nAP50       | nAP75       |             |
| FSRW (Kang et al., 2019)              | -        | 5.6  | 12.3        | 4.6         | -           | 9.1  | 19          | 7.6         |             |
| Meta R-CNN (Yan et al., 2019)         | 5.2      | 6.1  | 19.1        | 6.6         | 7.1         | 9.9  | 25.3        | 10.8        |             |
| TFA (Wang et al., 2020)               | 33.9     | 10   | 19.2        | 9.2         | 34.5        | 13.5 | 24.9        | 13.2        |             |
| FSCE (Sun et al., 2021)               | -        | 11.9 | -           | 10.5        | -           | 16.4 | -           | 16.2        |             |
| Retentive RCNN (Fan et al., 2021)     | 39.2     | 10.5 | 19.5        | 9.3         | 39.3        | 13.8 | 22.9        | 13.8        |             |
| HeteroGraph (Han et al., 2021)        | -        | 11.6 | 23.9        | 9.8         | -           | 16.5 | 31.9        | 15.5        |             |
| FsDetView (Xiao et al., 2022)         | 6.4      | 7.6  | -           | -           | 9.3         | 12   | -           | -           |             |
| Meta Faster R-CNN (Han et al., 2022a) | -        | 12.7 | 25.7        | 10.8        | -           | 16.6 | 31.8        | 15.8        |             |
| LVC (Kaul et al., 2022)               | 28.7     | 19   | 34.1        | 19          | 34.8        | 26.8 | 45.8        | 27.5        |             |
| Cross-Transformer (Han et al., 2022b) | -        | 17.1 | 30.2        | 17          | -           | 21.4 | 35.5        | 22.1        |             |
| NIFF (Guirguis et al., 2023)          | 39       | 18.8 | -           | -           | 39          | 20.9 | -           | -           |             |
| DiGeo (Ma et al., 2023)               | 39.2     | 10.3 | 18.7        | 9.9         | 39.4        | 14.2 | 26.2        | 14.8        |             |
| DE-ViT (Ours)                         | ViT-S/14 | 24   | <b>27.1</b> | <b>43.1</b> | <b>28.5</b> | 24.2 | <b>26.9</b> | <b>43.1</b> | <b>28.4</b> |
|                                       | ViT-B/14 | 28.3 | <b>33.2</b> | <b>51.4</b> | <b>35.5</b> | 28.5 | <b>33.4</b> | <b>51.4</b> | <b>35.7</b> |
|                                       | ViT-L/14 | 29.4 | <b>34.0</b> | <b>53.0</b> | <b>37.0</b> | 29.5 | <b>34.0</b> | <b>52.9</b> | <b>37.2</b> |

Table 4: Results on COCO one-shot benchmark.

|                                   | Seen        |             |             |             |             | Unseen  |             |             |             |             |
|-----------------------------------|-------------|-------------|-------------|-------------|-------------|---------|-------------|-------------|-------------|-------------|
|                                   | Split-1     | Split-2     | Split-3     | Split-4     | Avg         | Split-1 | Split-2     | Split-3     | Split-4     | Avg         |
| SiamMask (Michaelis et al., 2018) | 38.9        | 37.1        | 37.8        | 36.6        | 37.6        | 15.3    | 17.6        | 17.4        | 17          | 16.8        |
| CoAE (Hsieh et al., 2019)         | 42.2        | 40.2        | 39.9        | 41.3        | 40.9        | 23.4    | 23.6        | 20.5        | 20.4        | 22          |
| AIT (Chen et al., 2021)           | 50.1        | 47.2        | 45.8        | 46.9        | 47.5        | 26      | 26.4        | 22.3        | 22.6        | 24.3        |
| SaFT (Zhao et al., 2022b)         | 49.2        | 47.2        | 47.9        | 49          | 48.3        | 27.8    | 27.6        | 21          | 23          | 24.9        |
| BHRL (Yang et al., 2022)          | 56          | 52.1        | 52.6        | 53.4        | 53.6        | 26.1    | 29          | 22.7        | 24.5        | 25.6        |
| DE-ViT (Ours, ViT-L/14)           | <b>59.4</b> | <b>57.0</b> | <b>61.3</b> | <b>60.7</b> | <b>59.6</b> | 27.4    | <b>33.2</b> | <b>27.1</b> | <b>26.1</b> | <b>28.4</b> |

## 4.2 ANALYSIS

**Efficiency.** In Tab. 5 and 6, we compare the efficiency of DE-ViT against previous SoTA open-vocabulary methods. We study the effects of selecting different numbers of classes ( $K$ ) during class preselection. The inference speed is measured under PyTorch 1.13 with one A100 GPU, except for OWL-ViT which is implemented in JAX framework (Frostig et al., 2018). DE-ViT outperforms SoTA while being much faster at COCO and slightly slower at LVIS when  $K = 3$ . Note that JAX is commonly known as faster than pytorch (Phan et al., 2019). Our main results are obtained using  $K = 10$ . We select CORA instead of CORA<sup>+</sup> and OWL-ViT rather than Ro-ViT for comparison because the latter implementations have not been released at the moment this paper is written. Note



Table 5: Efficiency comparison against existing state-of-the-art on COCO OVD benchmark.

| Method           | Backbone | top $K$ | Novel AP50 | Secs/Img |
|------------------|----------|---------|------------|----------|
| DE-ViT<br>(Ours) | ViT-L/14 | 1       | 47.7       | 0.22     |
|                  |          | 3       | 50.0       | 0.33     |
|                  |          | 10      | 50.0       | 0.83     |
| CORA             | RN50x4   | -       | 41.7       | 0.5      |

Table 6: Efficiency comparison against existing state-of-the-art on LVIS OVD benchmark.

| Method           | Backbone              | top $K$ | box AP <sub>r</sub> | Secs/Img |
|------------------|-----------------------|---------|---------------------|----------|
| DE-ViT<br>(Ours) | ViT-L/14<br>(pytorch) | 1       | 25.4                | 0.35     |
|                  |                       | 3       | 32.6                | 0.5      |
|                  |                       | 10      | 33.6                | 1.58     |
| OWL-ViT          | ViT-L/14 (jax)        | -       | 31.2                | 0.42     |

Table 7: Ablation studies on the classification architecture.

| Conventional<br>CLS Head | Prototype<br>Projection | Background<br>Tokens | Class<br>Rearrange | Novel |      | Base |      |
|--------------------------|-------------------------|----------------------|--------------------|-------|------|------|------|
|                          |                         |                      |                    | AP50  | AP75 | AP50 | AP75 |
| ✓                        |                         |                      |                    | 4.5   | 2.2  | 48.9 | 22.5 |
|                          | ✓                       |                      |                    | 26.2  | 9.7  | 29.3 | 12   |
|                          | ✓                       | ✓                    |                    | 38.4  | 23   | 43.4 | 26.8 |
|                          | ✓                       | ✓                    | ✓                  | 39.5  | 24.1 | 42.3 | 25.9 |

Table 8: Ablation studies on annotation types used to build prototypes.

| Support Images<br>Annotation | nAP50  |         |         |
|------------------------------|--------|---------|---------|
|                              | 5-shot | 10-shot | 30-shot |
| mask                         | 43.1   | 43.1    | 43.1    |
| bbox                         | 43     | 42.6    | 43.1    |

that we use half-precision for ViT inference as the standard practice for vision transformers, and full precision for other layers. We choose open-vocabulary over few-shot methods for comparison because of their superior accuracy.

**Feature Visualization of DINOv2 and CLIP.** The critical distinction between DE-ViT and OVD methods is that DE-ViT uses visual features and represents each class by the center of visual features, while OVD methods represent each class with text features, mostly from CLIP. Therefore, we sample and visualize DINOv2 and CLIP features in Fig. A2 using UMap (McInnes et al., 2018). CLIP visual features also show excellent intra-class compactness. However, there is a huge vacuum between CLIP text and visual features, and text features are almost overlapped with each other. This indicates that the distances between text and visual features may be more susceptible to noises. This further suggests that using images to represent classes could be more promising than only using texts.

### 4.3 ABLATION STUDY

**Classification.** We examine the component effects for classification in Tab. 7. For the conventional CLS head, we follow an architecture similar to RegionCLIP that inputs features to the RCNN head and composes the last linear layer with class prototypes. Tab. 7 shows that the model completely overfits base classes without our proposed components. By learning from similarity maps from prototype projection, general detection ability emerges, and then improves after adding the background prototypes and the class rearrange module. Results in Tab. 7, 9 and 8 are obtained with ViT-S/14.

**Refined Localization.** We study the impacts of region propagation in Tab. 9. For the conventional REG head, we use a CNN with both features and similarity maps as input. Novel classes have poor localization

(14.6 AP75) without our proposed architecture, and simply expanding proposals even lowers the performance. The localization accuracy jumps to 24.1 AP75 when the heatmap representation is used with spatial integrals to produce bounding boxes.

**Using Boxes or Masks to Build Prototypes.** In Tab. 8, we study the effects of annotation types, *i.e.*, bounding boxes or masks, in constructing prototypes. We observe that using bounding boxes to build prototypes yields almost indistinguishable performance compared to using instance masks at even 5-shot. Our main results use prototypes built from instance masks.

## 5 CONCLUSION

Our method has shown positive results in using images as the category representation in an open-set object detector. Since our method detects objects using only frozen visual features, it is straightforward to integrate DE-ViT with more backbones or co-exist with networks for other downstream tasks. Some limitations are still to be investigated. (1) Using only one prototype per class is a bottle-

Table 9: Ablation studies on the refined localization pipeline.

| Conventional<br>REG Head | Expanded<br>Proposal | Spatial Integral<br>over Heatmap | Novel |      | Base |      |
|--------------------------|----------------------|----------------------------------|-------|------|------|------|
|                          |                      |                                  | AP50  | AP75 | AP50 | AP75 |
| ✓                        |                      |                                  | 37.7  | 14.6 | 46.5 | 23.9 |
| ✓                        | ✓                    |                                  | 35.6  | 12.5 | 41.3 | 19.8 |
|                          | ✓                    | ✓                                | 39.5  | 24.1 | 42.3 | 25.9 |

neck representation and prohibits complex spatial reasoning. (2) We apply a hybrid ViT and RCNN structure while a full transformer network could be conceptually more scalable and performant. (3) The ViT backbone is frozen to retain generalization power that would be lost otherwise. This issue remains unresolved. (4) Our implementation depends on a ResNet RPN, which introduces extra computation costs and may limit detection recall. This issue could be solved with some engineering efforts, e.g., training RPN on top of ViT, or re-purposing our localization module for RPN. We hope that our work will be useful in downstream tasks such as robotic manipulation, and help other researchers develop better methods for open-vocabulary and few-shot object detection.

## REFERENCES

- Simone Antonelli, Danilo Avola, Luigi Cinque, Donato Crisostomi, Gian Luca Foresti, Fabio Galasso, Marco Raoul Marini, Alessio Mecca, and Daniele Pannone. Few-shot object detection: A survey. *ACM Computing Surveys (CSUR)*, 54(11s):1–37, 2022.
- Holger Caesar, Jasper Uijlings, and Vittorio Ferrari. Coco-stuff: Thing and stuff classes in context. In *Proceedings of the IEEE Conference on Computer Vision and Pattern Recognition*, pp. 1209–1218, 2018.
- Berk Calli, Arjun Singh, Aaron Walsman, Siddhartha Srinivasa, Pieter Abbeel, and Aaron M Dollar. The ycb object and model set: Towards common benchmarks for manipulation research. In *International Conference on Advanced Robotics (ICAR)*, pp. 510–517. IEEE, 2015.
- Nicolas Carion, Francisco Massa, Gabriel Synnaeve, Nicolas Usunier, Alexander Kirillov, and Sergey Zagoruyko. End-to-end object detection with transformers. In *European Conference on Computer Vision*, pp. 213–229. Springer, 2020.
- Mathilde Caron, Ishan Misra, Julien Mairal, Priya Goyal, Piotr Bojanowski, and Armand Joulin. Unsupervised learning of visual features by contrasting cluster assignments. *Advances in Neural Information Processing Systems*, 33:9912–9924, 2020.
- Ding-Jie Chen, He-Yen Hsieh, and Tyng-Luh Liu. Adaptive image transformer for one-shot object detection. In *Proceedings of the IEEE/CVF Conference on Computer Vision and Pattern Recognition*, pp. 12247–12256, 2021.
- Peixian Chen, Kekai Sheng, Mengdan Zhang, Yunhang Shen, Ke Li, and Chunhua Shen. Open vocabulary object detection with proposal mining and prediction equalization. *arXiv preprint arXiv:2206.11134*, 2022.
- Xinlei Chen, Hao Fang, Tsung-Yi Lin, Ramakrishna Vedantam, Saurabh Gupta, Piotr Dollár, and C Lawrence Zitnick. Microsoft coco captions: Data collection and evaluation server. *arXiv preprint arXiv:1504.00325*, 2015.
- Han-Cheol Cho, Won Young Jhoo, Wooyoung Kang, and Byungseok Roh. Open-vocabulary object detection using pseudo caption labels. *arXiv preprint arXiv:2303.13040*, 2023.
- Marco Cuturi. Sinkhorn distances: Lightspeed computation of optimal transport. *Advances in Neural Information Processing Systems*, 26, 2013.
- Sergey N Dorogovtsev and José Fernando F Mendes. Language as an evolving word web. *Proceedings of the Royal Society of London. Series B: Biological Sciences*, 268(1485):2603–2606, 2001.
- Zhibo Fan, Yuchen Ma, Zeming Li, and Jian Sun. Generalized few-shot object detection without forgetting. In *Proceedings of the IEEE/CVF Conference on Computer Vision and Pattern Recognition*, pp. 4527–4536, 2021.
- Roy Frostig, Matthew James Johnson, and Chris Leary. Compiling machine learning programs via high-level tracing. *Systems for Machine Learning*, 4(9), 2018.
- Ross Girshick. Fast r-cnn. In *Proceedings of the IEEE International Conference on Computer Vision*, pp. 1440–1448, 2015.

- Xiuye Gu, Tsung-Yi Lin, Weicheng Kuo, and Yin Cui. Open-vocabulary object detection via vision and language knowledge distillation. In *International Conference on Learning Representations*, 2021.
- Karim Guirguis, Johannes Meier, George Eskandar, Matthias Kayser, Bin Yang, and Jürgen Beyrer. Niff: Alleviating forgetting in generalized few-shot object detection via neural instance feature forging. In *Proceedings of the IEEE/CVF Conference on Computer Vision and Pattern Recognition*, pp. 24193–24202, 2023.
- Agrim Gupta, Piotr Dollar, and Ross Girshick. Lvis: A dataset for large vocabulary instance segmentation. In *Proceedings of the IEEE/CVF Conference on Computer Vision and Pattern Recognition*, pp. 5356–5364, 2019.
- Guangxing Han, Yicheng He, Shiyuan Huang, Jiawei Ma, and Shih-Fu Chang. Query adaptive few-shot object detection with heterogeneous graph convolutional networks. In *Proceedings of the IEEE/CVF International Conference on Computer Vision*, pp. 3263–3272, 2021.
- Guangxing Han, Shiyuan Huang, Jiawei Ma, Yicheng He, and Shih-Fu Chang. Meta faster r-cnn: Towards accurate few-shot object detection with attentive feature alignment. In *Proceedings of the AAAI Conference on Artificial Intelligence*, volume 36, pp. 780–789, 2022a.
- Guangxing Han, Jiawei Ma, Shiyuan Huang, Long Chen, and Shih-Fu Chang. Few-shot object detection with fully cross-transformer. In *Proceedings of the IEEE/CVF Conference on Computer Vision and Pattern Recognition*, pp. 5321–5330, 2022b.
- Kaiming He, Georgia Gkioxari, Piotr Dollár, and Ross Girshick. Mask r-cnn. In *Proceedings of the IEEE International Conference on Computer Vision*, pp. 2961–2969, 2017.
- Ting-I Hsieh, Yi-Chen Lo, Hwann-Tzong Chen, and Tyng-Luh Liu. One-shot object detection with co-attention and co-excitation. *Advances in Neural Information Processing Systems*, 32, 2019.
- Jie Hu, Li Shen, and Gang Sun. Squeeze-and-excitation networks. In *Proceedings of the IEEE Conference on Computer Vision and Pattern Recognition*, pp. 7132–7141, 2018.
- Tomas Jakab, Ankush Gupta, Hakan Bilen, and Andrea Vedaldi. Unsupervised learning of object landmarks through conditional image generation. *Advances in Neural Information Processing Systems*, 31, 2018.
- Bingyi Kang, Zhuang Liu, Xin Wang, Fisher Yu, Jiashi Feng, and Trevor Darrell. Few-shot object detection via feature reweighting. In *Proceedings of the IEEE/CVF International Conference on Computer Vision*, pp. 8420–8429, 2019.
- Prannay Kaul, Weidi Xie, and Andrew Zisserman. Label, verify, correct: A simple few shot object detection method. In *Proceedings of the IEEE/CVF Conference on Computer Vision and Pattern Recognition*, pp. 14237–14247, 2022.
- Dahun Kim, Anelia Angelova, and Weicheng Kuo. Region-aware pretraining for open-vocabulary object detection with vision transformers. In *Proceedings of the IEEE/CVF Conference on Computer Vision and Pattern Recognition*, pp. 11144–11154, 2023.
- Mona Köhler, Markus Eisenbach, and Horst-Michael Gross. Few-shot object detection: a comprehensive survey. *IEEE Transactions on Neural Networks and Learning Systems*, 2023.
- Alex Krizhevsky, Ilya Sutskever, and Geoffrey E Hinton. Imagenet classification with deep convolutional neural networks. *Advances in Neural Information Processing Systems*, 25, 2012.
- Tejas D Kulkarni, Ankush Gupta, Catalin Ionescu, Sebastian Borgeaud, Malcolm Reynolds, Andrew Zisserman, and Volodymyr Mnih. Unsupervised learning of object keypoints for perception and control. *Advances in Neural Information Processing Systems*, 32, 2019.
- Barbara Landau, Lila R Gleitman, and Barbara Landau. *Language and experience: Evidence from the blind child*, volume 8. Harvard University Press, 2009.

- Tsung-Yi Lin, Michael Maire, Serge Belongie, James Hays, Pietro Perona, Deva Ramanan, Piotr Dollár, and C Lawrence Zitnick. Microsoft coco: Common objects in context. In *European Conference on Computer Vision*, pp. 740–755. Springer, 2014.
- Qin Liu, Zhenlin Xu, Gedas Bertasius, and Marc Niethammer. Simpleclick: Interactive image segmentation with simple vision transformers. *arXiv preprint arXiv:2210.11006*, 2022.
- Shilong Liu, Zhaoyang Zeng, Tianhe Ren, Feng Li, Hao Zhang, Jie Yang, Chunyuan Li, Jianwei Yang, Hang Su, Jun Zhu, et al. Grounding dino: Marrying dino with grounded pre-training for open-set object detection. *arXiv preprint arXiv:2303.05499*, 2023.
- Jiawei Ma, Yulei Niu, Jincheng Xu, Shiyuan Huang, Guangxing Han, and Shih-Fu Chang. Digeo: Discriminative geometry-aware learning for generalized few-shot object detection. In *Proceedings of the IEEE/CVF Conference on Computer Vision and Pattern Recognition*, pp. 3208–3218, 2023.
- Leland McInnes, John Healy, and James Melville. Umap: Uniform manifold approximation and projection for dimension reduction. *arXiv preprint arXiv:1802.03426*, 2018.
- Claudio Michaelis, Ivan Ustyuzhaninov, Matthias Bethge, and Alexander S Ecker. One-shot instance segmentation. *arXiv preprint arXiv:1811.11507*, 2018.
- Matthias Minderer, Alexey Gritsenko, Austin Stone, Maxim Neumann, Dirk Weissenborn, Alexey Dosovitskiy, Aravindh Mahendran, Anurag Arnab, Mostafa Dehghani, Zhuoran Shen, et al. Simple open-vocabulary object detection. In *European Conference on Computer Vision*, pp. 728–755. Springer, 2022.
- Atsuro Okazawa. Interclass prototype relation for few-shot segmentation. In *European Conference on Computer Vision*, pp. 362–378. Springer, 2022.
- Maxime Oquab, Timothée Darcet, Théo Moutakanni, Huy Vo, Marc Szafraniec, Vasil Khalidov, Pierre Fernandez, Daniel Haziza, Francisco Massa, Alaaeldin El-Nouby, et al. Dinov2: Learning robust visual features without supervision. *arXiv preprint arXiv:2304.07193*, 2023.
- Du Phan, Neeraj Pradhan, and Martin Jankowiak. Composable effects for flexible and accelerated probabilistic programming in numpyro. *arXiv preprint arXiv:1912.11554*, 2019.
- Telmo Pires, Eva Schlinger, and Dan Garrette. How multilingual is multilingual bert? *arXiv preprint arXiv:1906.01502*, 2019.
- Alec Radford, Jong Wook Kim, Chris Hallacy, Aditya Ramesh, Gabriel Goh, Sandhini Agarwal, Girish Sastry, Amanda Askell, Pamela Mishkin, Jack Clark, et al. Learning transferable visual models from natural language supervision. In *International Conference on Machine Learning*, pp. 8748–8763. PMLR, 2021.
- Carole H Sudre, Wenqi Li, Tom Vercauteren, Sebastien Ourselin, and M Jorge Cardoso. Generalised dice overlap as a deep learning loss function for highly unbalanced segmentations. In *Deep Learning in Medical Image Analysis and Multimodal Learning for Clinical Decision Support: Third International Workshop*, pp. 240–248. Springer, 2017.
- Bo Sun, Banghuai Li, Shengcai Cai, Ye Yuan, and Chi Zhang. Fsce: Few-shot object detection via contrastive proposal encoding. In *Proceedings of the IEEE/CVF Conference on Computer Vision and Pattern Recognition*, pp. 7352–7362, 2021.
- Cédric Villani et al. *Optimal transport: old and new*, volume 338. Springer, 2009.
- Wenguan Wang, Cheng Han, Tianfei Zhou, and Dongfang Liu. Visual recognition with deep nearest centroids. *arXiv preprint arXiv:2209.07383*, 2022.
- Xin Wang, Thomas E Huang, Trevor Darrell, Joseph E Gonzalez, and Fisher Yu. Frustratingly simple few-shot object detection. *arXiv preprint arXiv:2003.06957*, 2020.
- Jianzong Wu, Xiangtai Li, Shilin Xu Haobo Yuan, Henghui Ding, Yibo Yang, Xia Li, Jiangning Zhang, Yunhai Tong, Xudong Jiang, Bernard Ghanem, et al. Towards open vocabulary learning: A survey. *arXiv preprint arXiv:2306.15880*, 2023a.

- Size Wu, Wenwei Zhang, Sheng Jin, Wentao Liu, and Chen Change Loy. Aligning bag of regions for open-vocabulary object detection. In *Proceedings of the IEEE/CVF Conference on Computer Vision and Pattern Recognition*, pp. 15254–15264, 2023b.
- Xiaoshi Wu, Feng Zhu, Rui Zhao, and Hongsheng Li. Cora: Adapting clip for open-vocabulary detection with region prompting and anchor pre-matching. In *Proceedings of the IEEE/CVF Conference on Computer Vision and Pattern Recognition*, pp. 7031–7040, 2023c.
- Yang Xiao, Vincent Lepetit, and Renaud Marlet. Few-shot object detection and viewpoint estimation for objects in the wild. *IEEE Transactions on Pattern Analysis and Machine Intelligence*, 45(3): 3090–3106, 2022.
- Xiaopeng Yan, Ziliang Chen, Anni Xu, Xiaoxi Wang, Xiaodan Liang, and Liang Lin. Meta r-cnn: Towards general solver for instance-level low-shot learning. In *Proceedings of the IEEE/CVF International Conference on Computer Vision*, pp. 9577–9586, 2019.
- Hanqing Yang, Sijia Cai, Hualian Sheng, Bing Deng, Jianqiang Huang, Xian-Sheng Hua, Yong Tang, and Yu Zhang. Balanced and hierarchical relation learning for one-shot object detection. In *Proceedings of the IEEE/CVF Conference on Computer Vision and Pattern Recognition*, pp. 7591–7600, 2022.
- Yuhang Zang, Wei Li, Kaiyang Zhou, Chen Huang, and Chen Change Loy. Open-vocabulary det with conditional matching. In *European Conference on Computer Vision*, pp. 106–122. Springer, 2022.
- Alireza Zareian, Kevin Dela Rosa, Derek Hao Hu, and Shih-Fu Chang. Open-vocabulary object detection using captions. In *Proceedings of the IEEE/CVF Conference on Computer Vision and Pattern Recognition*, pp. 14393–14402, 2021.
- Shiyu Zhao, Zhixing Zhang, Samuel Schuster, Long Zhao, BG Vijay Kumar, Anastasis Stathopoulos, Manmohan Chandraker, and Dimitris N Metaxas. Exploiting unlabeled data with vision and language models for object detection. In *European Conference on Computer Vision*, pp. 159–175. Springer, 2022a.
- Yizhou Zhao, Xun Guo, and Yan Lu. Semantic-aligned fusion transformer for one-shot object detection. In *Proceedings of the IEEE/CVF Conference on Computer Vision and Pattern Recognition*, pp. 7601–7611, 2022b.
- Yiwu Zhong, Jianwei Yang, Pengchuan Zhang, Chunyuan Li, Noel Codella, Liunian Harold Li, Luowei Zhou, Xiyang Dai, Lu Yuan, Yin Li, et al. Regionclip: Region-based language-image pretraining. In *Proceedings of the IEEE/CVF Conference on Computer Vision and Pattern Recognition*, pp. 16793–16803, 2022.
- Tianfei Zhou, Wenguan Wang, Ender Konukoglu, and Luc Van Gool. Rethinking semantic segmentation: A prototype view. In *Proceedings of the IEEE/CVF Conference on Computer Vision and Pattern Recognition*, pp. 2582–2593, 2022a.
- Xingyi Zhou, Rohit Girdhar, Armand Joulin, Philipp Krähenbühl, and Ishan Misra. Detecting twenty-thousand classes using image-level supervision. In *European Conference on Computer Vision*, pp. 350–368. Springer, 2022b.

## A APPENDIX

### A.1 VISUALIZATION DETAILS

**Demonstration on YCB Objects.** Fig. 1 shows the detection results of DE-ViT on YCB objects, a standard set of objects widely used in robotic manipulation benchmark (Calli et al., 2015). There are misclassifications and inaccurate boxes, *e.g.*, the white skillet is mistaken as a can, all round-shape fruits are recognized as orange, while the red one is clearly an apple. However, we believe the overall result is encouraging. The specification of YCB objects at the time this paper is written includes 72 categories. We use a total of 33 by selecting and merging certain categories. The categories in use are apple, ball, banana, bowl, brick, can, cheez-it, chips, clamp, cleanser bottle, coffee jar, comet pine, cups, drill, glass, lego, lemon, marker, mug, mustard, orange, peach, pear, peg-hole, pitcher, plate, screwdriver, skillet, spray bottle, sugar box, toy airplane box, utensil, wood blocks jar. The source image in Fig. 1 is taken from the banner picture of [ycbbenchmarks.com](http://ycbbenchmarks.com). For each category, we use google image search to collect a few sample images. Fewer than four images on average are gathered per category. We annotate the corresponding objects by instance masks in each image using the software provided by SimpleClick (Liu et al., 2022). Similar to SAM, SimpleClick generates instance masks automatically from user clicks, which significantly simplifies and accelerates the annotation procedure. Our annotator feedback indicates that annotating masks with SimpleClick is even easier and more accurate than drawing bounding boxes. An NVIDIA 3060 GPU is used for SimpleClick software. Class prototypes for YCB objects are built from the annotated example images. During DE-ViT inference, we replace prototypes of LVIS categories with those of YCB objects in order to detect these new categories. During postprocessing, We apply class-agnostic NMS and filter small bounding boxes. The full code and data for this demonstration will be released in our repository.



Figure A1: Examples of heatmaps in region propagation. The proposal, expanded proposal, and final prediction box are colored in red, pink, and yellow, respectively. The initial heatmap encodes the spatial relationship between proposals and expanded proposals in binary masks. Propagated heatmaps are softmax predictions sampled from the binary segmentation network in our region propagation architecture.

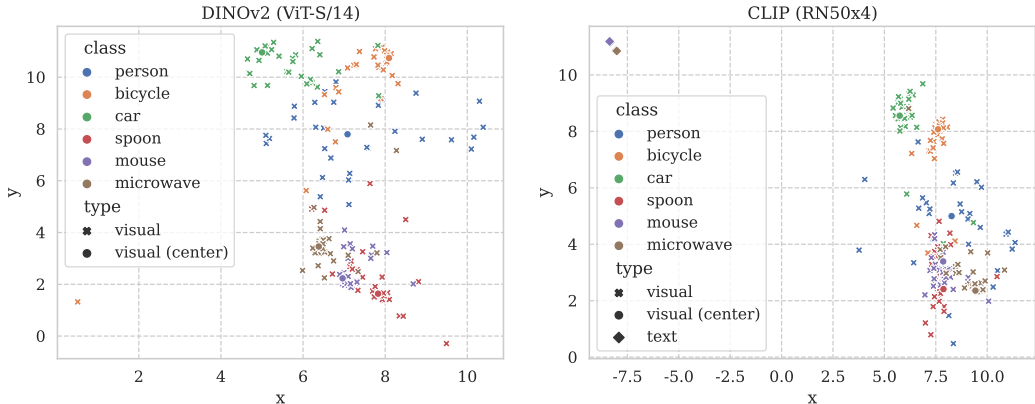


Figure A2: Visualization of DINOv2 and CLIP (RN50x4) features in 2d plane. From visual features ( $\star$ ), both DINOv2 and CLIP show good concentration within each class. However, CLIP text features ( $\blacklozenge$ ) locate much further from visual features. In contrast to centers of visual features ( $\bullet$ ), text features of different classes overlap each other, showing much smaller inter-class distances.

**Feature Visualization of DINOv2 and CLIP.** Fig. A2 visualizes the features of DINOv2 and CLIP, as we discussed in Sec. 4.2. Visual features of DINOv2 are extracted using groundtruth bounding boxes with the procedure shown in Fig. 5. For CLIP, we follow the standard text and region visual features extraction procedure (Zhong et al., 2022; Wu et al., 2023c). Specifically, visual features are obtained by applying ROIAlign on the output of `res4` block. The ROIAlign outputs are fed into `res5` and attention pooling blocks to produce the final feature vector. Text features are extracted with CLIP text encoders with category names. We randomly sample 30 instances per class for visualization, *i.e.*, each node (✖) represents an instance of the corresponding class. The UMap dimension reduction transformation is learned with a larger set of instances with both visual and text features.

**Region Propagation.** Fig. A1 visualizes the heatmap changes of sampled detection results during region propagation. A clear mapping can be found between the detection bounding boxes and the corresponding salient regions within the expanded proposal. The softmax predictions are normalized by dividing mean values in order to enhance the visual quality.

## A.2 DISCUSSION

We highlight that the parameters introduced by our classification and localization network only occupy a small fraction compared to the ViT backbone, *e.g.*, 7.7M versus 304M for COCO ViT-L/14. Moreover, the similar visual feature distribution of DINOv2 and CLIP shown in Fig. A2 also suggests that our method may apply to other backbones besides DINOv2 ViTs. Considering that our method detects objects from frozen visual features, it could be seen as a pipeline that extracts object information from visual features, similar to the linear probe protocol for semantic segmentation (Oquab et al., 2023).

Despite having strong results, one limitation of DE-ViT is the bottlenecked representation of one prototype per class. In contrast to some recent few-shot methods like CrossTransformer (Han et al., 2022b) that applies dense feature interaction between support and input images, our method represents each class by a single prototype vector, which enables a simplified framework and better efficiency. However, there are cases when more expensive spatial reasoning becomes necessary, such as when certain categories share a similar appearance or have specific shapes. This further leads to the architectural limitation of DE-ViT. Our method uses a hybrid structure with ViT backbone and RCNN head, while a full transformer network shall be conceptually more performant and scalable. Moreover, as mentioned in Sec. 3.2 and shown in Tab. 7, the ViT backbone is kept frozen to retain the generalization power which would be lost otherwise during finetuning. This could be viewed as our unresolved issue for using images as category representation.

Another limitation is that our current implementation relies on a ResNet50 RPN network, which introduces extra computational overhead and may even limit the detection recall. This issue should be able to resolve with some engineering efforts, such as training an RPN head on top of the ViT backbone or repurposing our localization architectures for RPN by doing refined localizations over a set of pre-defined boxes. The anchor pre-matching technique in the framework of CORA is similar to the latter strategy.

## A.3 IMPLEMENTATION DETAILS

### A.3.1 NETWORK ARCHITECTURE

Fig. A3 illustrates the network building block used in our convolution neural networks for classification, localization, and instance segmentation branches. Sigmoid cross entropy loss and dice loss (Sudre et al., 2017) are applied on the mask output at each layer in the localization and segmentation branch. The red blocks are only used in the classification branch. For the classification branch, the mask prediction serves as spatial attention and receives no supervision, similar to the squeeze-and-excitation block in SENet (Hu et al., 2018) but at spatial dimensions. The input to both classification and localization branches is the similarity map between proposal features and prototypes, while the input to the instance segmentation branch for LVIS is the concatenation

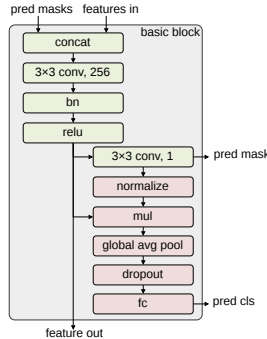


Figure A3: Basic building block for our RCNN networks.



of similarity maps and multi-scale ViT features. For models trained with COCO, we use 3 blocks for classification and 5 blocks for localization. For LVIS, we use 5 blocks for all branches. The  $3 \times 3 \text{ conv}_r, 256$  denotes a convolution layer with kernel size 3 and 256 output channels. We use  $T = 128$  in the class rearrange module for both COCO and LVIS.

### A.3.2 OPERATIONS

**Proposal Expansion.** Eq. 6 explains the proposal expansion block in Fig. 4.  $(c_w, c_h, w, h)$  and  $(c_w^{\text{exp}}, c_h^{\text{exp}}, w^{\text{exp}}, h^{\text{exp}})$  represent the original the expanded proposal.

$$\begin{aligned} m &= \min(0.4w, 0.4h) \\ (w^{\text{exp}}, h^{\text{exp}}) &= (w, h) + m \\ (c_w^{\text{exp}}, c_h^{\text{exp}}) &= (c_w, c_h) \end{aligned} \quad (6)$$

**Box2Heatmap.** Eq. 7 explains the Box2Heatmap block in Fig. 4.  $\mathbf{H} \in \mathbb{R}^{H \times W}$  represents the output heatmap.  $(x_0, y_0)$  and  $(x_1, y_1)$  denotes the coordinates of the left top and right bottom point of the original proposal, where  $(x_0, y_0) = (c_w, c_h) - (w, h)/2$  and  $(x_1, y_1) = (c_w, c_h) + (w, h)/2$ .

$$\mathbf{H}_{ji} = \begin{cases} 1 & (x_0^{\text{exp}} + \frac{i}{W}w^{\text{exp}}, y_0^{\text{exp}} + \frac{j}{H}h^{\text{exp}}) \in [x_0, x_1] \times [y_0, y_1] \\ 0 & \text{otherwise} \end{cases} \quad (7)$$

**Clustering.** The clustering algorithm used in building prototypes is initially proposed by SwAV (Caron et al., 2020) and based on optimal transport (Villani et al., 2009). The optimal transport problem is an optimization problem that aims to find an optimal mapping  $\gamma^* \in \mathbb{R}_+^{n \times m}$  from a source distribution  $\mathbf{a} = [a_1, \dots, a_n]$ ,  $\sum_{i=1}^n a_i = 1$  to target distribution  $\mathbf{b} = [b_1, \dots, b_n]$ ,  $\sum_{i=1}^m b_i = 1$ , which minimizes the overall transport cost. Let  $\mathbf{M} \in \mathbb{R}^{n \times m}$  denote the cost matrix, where  $\mathbf{M}_{ij}$  denote the cost of moving mass from  $a_i$  to  $b_j$ . This problem is formulated in Eq. 8.

$$\begin{aligned} \gamma^* &= \arg \min_{\gamma \in \mathbb{R}_+^{n \times m}} \sum_{i,j} \gamma_{ij} \mathbf{M}_{ij} \\ \text{s.t. } &\gamma \mathbf{1} = \mathbf{a}; \gamma^T \mathbf{1} = \mathbf{b}; \gamma \geq 0 \end{aligned} \quad (8)$$

The clustering procedure consists of the iterations of two steps. First, an optimal transport  $\gamma^*$  is computed between a set of centroids  $\mathbf{C} \in \mathbb{R}^{c \times d}$  and instance-level prototypes  $\mathbf{Q} \in \mathbb{R}^{q \times d}$ , where  $c$  represents the number of centroids and  $q$  represents the number of instance-level prototypes for a given class in a mini-batch. Note that we apply data augmentation to generate more instance-level prototypes from a limited set of support images. The negative dot similarity  $\mathbf{M} = -\mathbf{C}\mathbf{Q}^T$  is used as the cost matrix, and  $\mathbf{a}, \mathbf{b}$  are set as uniform. The solution  $\gamma^*$  is estimated from the sinkhorn knopp algorithm (Cuturi, 2013). Second, a momentum update is made to the centroids with  $\mathbf{C} = (1 - \beta)\mathbf{C} + \beta\gamma^*\mathbf{Q}$ , where  $\beta$  is the momentum parameter. Clustering is applied on instance prototypes per class. We use  $c = 10$  and  $\beta = 0.002$  for all experiments and compute the average of the 10 centroids as the prototype for each class. For background prototypes, we directly use centroids without averaging. This optimal-transport-based online clustering procedure is commonly used in prototype learning (Zhou et al., 2022a; Wang et al., 2022). In hindsight, we also try directly setting class-level prototypes as the mean of instance prototypes for each class without augmentation. This yields almost identical results on open-vocabulary experiments for both COCO and LVIS with ViT-L/14, other settings are not tested. This suggests that the details of the clustering procedure may not be a critical element within our method.

### A.4 COMPARISON OF LVIS RESULTS IN FEW-SHOT OBJECT DETECTION

LVIS has been regarded as a highly challenging dataset for few-shot object detection (Wang et al., 2020). To the best of our knowledge, only DiGeo reports few-shot results on LVIS v1. Note that TFA (Wang et al., 2020) reports their results on LVIS v0.5, which is deprecated and no longer distributed. Tab. A1 shows that our method outperforms DiGeo in all metrics.

Table A1: Performance comparison with existing few-shot object methods on LVIS dataset. We report box AP as evaluation metrics.

| Method                  | APr      | APc         | APf         | AP          |             |
|-------------------------|----------|-------------|-------------|-------------|-------------|
| DiGeo (Ma et al., 2023) | 16.6     | 22.8        | 28          | 24.4        |             |
| DE-ViT (Ours)           | ViT-S/14 | <b>23.4</b> | 22.8        | 22.5        | 22.8        |
|                         | ViT-B/14 | <b>26.8</b> | <b>26.5</b> | 25.3        | <b>26</b>   |
|                         | ViT-L/14 | <b>33.6</b> | <b>30.1</b> | <b>30.7</b> | <b>30.9</b> |